## Supplemental Methods

*Skeletal imaging.* All imaging and analysis was performed in a blinded fashion as described by our group previously (1-3). For *in vivo* μCT scanning, mice were anesthetized (2% isoflurane in $O_2$) and maintained in an immobile state using a customized holder to prevent motion artifact and ensure consistent positioning throughout the scans of the right tibia using an *in vivo* μCT system (Viva Scan 40 μCT scanner, Scanco Medical AG, Basserdorf, Switzerland). A 2D scout scan of the proximal metaphysis of the tibia was performed to determine the scan region of interest immediately prior to each scan. Subsequently, the region distal to the growth plate was scanned to permit a 100 slice analysis of the proximal metaphysis, whereas a 50 slice region proximal to the tibiofibular junction was scanned for analysis of the diaphysis. At study Endpoint, *ex vivo* quantitative analyses of bone microarchitecture of the right tibia (proximal metaphysis/mid-shaft diaphysis) and lumbar vertebrae ($L_5$) were performed, as described (1-3). Scan settings were as follows: 55 kVp, 10.5 μm voxel size, 21.5 diameter, 145mA, 300 ms integration time. μCT parameters were derived using the manufacturer's protocols. Trabecular bone volume fraction (BV/TV; %) was assessed at the lumbar spine (200 slices) and proximal metaphysis (100 slices) of the right tibia. Further, at the proximal metaphysis (50 slices) and mid-diaphysis (50 slices) of the right tibia, cortical volumetric bone mineral density (Ct.vBMD; mg/cm$^3$), cortical thickness (Ct.Th; mm), endocortical circumference (E.C; mm), and periosteal circumference (P.C; mm) were assessed. In addition, bone strength at the proximal metaphysis (50 slices) and mid-diaphysis (50 slices) of the right tibia was simulated via micro-finite element analysis (μFEA) to examine failure load (N) using the manufacturer's software (Scanco Medical AG, Basserdorf, Switzerland; Finite Element-Software Version 1.13), as described (1-3).

*Compression load testing.* Tests of compression loading were performed in a blinded fashion as described by our group previously (2). Preparation of the bones and testing was consistent with an established protocol (4). Briefly, the fourth lumbar vertebrae ($L_4$) was removed from the mice, dissected of soft tissues, and the intervertebral discs were cut off with a scalpel. Specimen height and major/minor diameters of the anterior body at the superior endplate were then measured using a digital caliper (Digimatic Absolute, Mitutoyo, Aurora, IL). The posterior elements were carefully resected using a forceps to hold and shield the anterior body while cutting the processes off using a stone grinding wheel on a rotary power tool. Vertebrae were soaked in PBS solution for at least five minutes prior to testing. Specimens were then placed between two parallel steel plates mounted to a servohydraulic mechanical testing frame (Model 858, MTS Systems, Eden Prairie, MN). To prevent bone specimens from slipping, plates were covered with fine grit sandpaper. Bones were compressed under displacement control at a rate of three mm/min until reaching their peak load while sampling data at 20 Hz. Following compression load testing, bone specimens were potted in poly-methyl-methacrylate (PMMA) and sectioned with a diamond saw to measure cross-sectional geometry digitally (ImageJ, NIH). The ultimate stress was calculated by dividing the peak force by the cross-sectional area (CSA), while the composite modulus of elasticity was determined from the slope of the linear region of the stress-strain curve. This test determines the stiffness (N/mm), ultimate load (N), and ultimate stress (MPa) of the bone.

*Three-point bend testing.* The right femur was excised from mice, muscle/connective tissues were removed, and the bone was stored in saline soaked gauze at -20°C for a direct test of biomechanical strength by three-point bending. A three-point bend fixture was mounted on a servo hydraulic mechanical testing frame (Model 858, MTS Systems, Eden Prairie, MN) instrumented with a 100-N capacity load cell (Model 3397-25, Leebow Products, Troy, MI). Femurs were mounted on supports spanning 7.5 mm. Point loading was applied to the femur mid-shaft allowing the bones to flex in the sagittal plane. Specimens were kept moist by irrigating them with PBS solution. Loading was applied under displacement control at a rate of 10 mm/min until fracture. Force and displacement data were sampled at 100 Hz. The peak load was quantified as was the work to fracture, defined by the area under the force

displacement curve (5). Stiffness (N/mm) was calculated from the linear region slope of the force displacement curve.

*Nano-indentation testing.* Nanoindentation testing was performed in a blinded fashion as described previously by our group (2). The third lumbar vertebrae ($L_3$) was removed from the mice and stored in saline soaked gauze at -20°C. Vertebrae were later stripped of soft tissues and embedded in PMMA resin blocks. Using a low-speed diamond saw, the bones were sectioned slightly above mid-height. Following bone sectioning, liquid PMMA was pressed into the surface to fill in any void spaces and allowed to set. Bone specimens were sectioned transversely again at mid-height, and manually polished using successively finer abrasive cloths, as detailed previously (2). Indentation specifications were as follows: 2 x 2 array with 15 μm spacing, loading rate of 500 μN/s, peak load of 2000 μN, and 60 s hold before unloading. The Oliver-Pharr model (6) was used to calculate reduced modulus (Er; GPa) and hardness (H; GPa). Four cortical sites (anterior, posterior, left/right lateral) and two trabecular sites were tested on each bone; measures were averaged over four indents of the array to generate a single value for each site. Values across all sites were averaged to generate an aggregate value for each vertebrae specimen.

*Reference point microindenation (RPI) testing.* The left femur was excised from the mice and the muscle/connective tissues were removed, followed by storage in saline soaked gauze at -20°C for biomaterial RPI testing. Hardness testing was conducted using a Biodent HFC system (Active Life Scientific, Santa Barbara, CA). The test design was similar to a previously established protocol (7). Femurs were submerged in a bath of PBS and gripped with a jig, allowing positioning of the bones with an adjustable linear stage. A linear array was tested on both the anterior and posterior sides of the femur. Each array was centered on the femur mid-shaft with indentations made at linear intervals of 1-mm. A 2-N maximum load was applied for 10 cycles at a frequency of 10 Hz. Bones were indented using a reference BP2 probe (Active Life Scientific, Santa Barbara, CA) that had a flat-bevel, 90° cono-spherical tip with a radius ≤5 μm. At the start of each test, three indentations were performed on a PMMA block that was used as a reference; Total Indentation Distance (TID) values of bone were normalized to the TID of PMMA. In addition, the average value from the 3$^{rd}$ to 20$^{th}$ cycle of loading slope (avLS) was assessed. Previous RPI studies have established that the avLS correlates with bone tissue age and that a worse avLS is an acceptable surrogate measure of fracture toughness properties, including crack growth initiation toughness ($K_{init}$) and overall resistance to crack propagation ($J_{init}$) (8). Thus, as a bone's avLS decreases, the bone itself becomes more susceptible to fracture.

*Skeletal histomorphometry assessments.* All bone histomorphometry analyses were performed in blinded fashion as previously described by our group (2). The non-decalcified right tibia was embedded in MMA and sectioned. For static analyses, sections were stained for tartrate-resistant acid phosphatase (TRAP) activity to evaluate osteoclast numbers per bone perimeter (N.Oc/B.Pm, /mm) or with Goldner's Trichrome stain to assess osteoblast numbers per bone perimeter (N.Ob/B.Pm, /mm). For dynamic fluorochrome analyses, mice were injected i.p. with Alizarin Red (0.1 mL/mouse, 7.5 mg/mL, Sigma-Aldrich, Saint Louis, MO) and calcein (0.1 mL/mouse, 2.5 mg/mL, Sigma-Aldrich, Saint Louis, MO) on days nine and two, respectively, prior to euthanasia. Unstained sections were used to evaluate mineral apposition rate (MAR, mcm/d) and bone formation rate per bone surface (BFR/BS, $mcm^3/mcm^2/d$). Histomorphometry measurements and calculations were conducted using the Osteomeasure Analysis system (Osteometrics, Atlanta, GA).

*Biochemical assays.* All biochemical assays were performed in blinded fashion. As noted previously, non-fasted glucose (mg/dL) measurements were obtained weekly from tail blood (taken by nicking the distal end of the tail) using a FreeStyle Lite glucose monitor (Cardinal Health Pharmacy, Hudson, WI). In addition to glucose, non-fasted HbA1c (%) was measured in tail blood at Baseline (age 4 months), Midpoint (age 5.5 months), and Endpoint (age 7 months) of the Experimental phase using the A1c Now+ System (Thermo Fisher Scientific, Wilmington, DE). At the same timepoints, non-fasted insulin (ng/mL)

levels were measured in plasma collected via lateral saphenous venipuncture using an ultrasensitive mouse Insulin ELISA kit (Alpco, Salem, NH). At study Endpoint, serum was collected in the morning (under non-fasting conditions) from anesthetized mice via cardiac puncture and stored at -80°C in aliquots for additional biochemical assays, which included circulating levels of bone turnover markers. More specifically, the serum bone formation marker P1NP (amino-terminal propeptide of type I collagen; ng/mL) was measured using the Rat/Mouse P1NP enzyme immunoassay (EIA) kit (interassay coefficient of variation [CV] <10%), whereas the serum bone resorption marker CTx (cross-linked C-telopeptide of type I collagen; ng/mL) was measured by the RatLaps Rat/Mouse CTx EIA kit (interassay CV <10%). Kits were purchased from Immuno Diagnostic Systems (IDS, Scottsdale, AZ).

*Quantification of advanced glycation endproducts (AGEs).* Measures of AGEs, including $N^{\varepsilon}$-(1-carboxymethyl)-L-Lysine (CML) and pentosidine in bone tissue samples and in non-fasted circulating serum samples were performed using mass spectrometry. The following reagents were obtained: CML (Toronto Research Chemicals), Nε-(1-carboxymethyl)-LLysine- d4 (CML-d4) (Toronto Research Chemicals), pentosidine (Cayman Chemicals), pentosidine-d3 trifluoroacetic acid salt (Toronto Research Chemicals), hydrochloric acid [HCL] (36.5-38.0%) (Sigma Aldrich), perfluoropentanoic acid (97%) (Sigma Aldrich), ammonium hydroxide (28-30%) (Sigma Aldrich), acetonitrile (Fisher Scientific), methanol (Fisher Scientific), and acetone (Fisher Scientific). Separate stock solutions (1 mg/mL) of CML and pentosidine were prepared followed by subsequent intermediate solutions in $H_2O$ (final concentrations of 100 µg/mL). Intermediate calibrators were serially diluted with $H_2O$ to generate a working calibration curve containing nine standards; CML and pentosidine ranged from 0–10,900 ng/mL and 0–800 ng/mL, respectively. Stock solutions (1 mg/mL) of deuterated internal standards, CML-d4 and Pentosidine-d3, were prepared, followed by working solutions of CML-d4 and pentosidine-d3 at 10 µg/mL and 1 µg/mL, respectively. Quality controls (QCs) were made from samples that were either undiluted, spiked with CML or pentosidine, or diluted with $H_2O$ thus creating samples that contained low, medium, and high analyte levels, respectively; QCs were run before and after each assay. All standards, controls, and samples were stored at -80°C. For hydrolysis of samples, 50 µL of control or sample was pipetted into 13×100 mm borosilicate glass culture tubes with 475 µL of 6 M HCl prepared in $H_2O$, 25 µL of 10 µg/mL CML-d4, and 25 µL of 1 µg/mL pentosidine-d3.

For the quantification of AGEs in serum, as described previously by our group (9), HCl (6M) was added to each standard, QC sample, and serum sample, followed by the addition of CML-d4 internal standard 10ug/ml and pentosidine-d3 internal standard 1ug/mL. Samples (divided into duplicates) were next brought to room temperature (RT), centrifuged at 3,000 rpm for 10 min, and then in order to extract analytes, 0.6 mLs of activated AG-50W-X8 resin (Bio-Rad Laboratories) was added to filter tubes, followed by five washes with nanopure $H_2O$. Hydrolysates were then transferred onto the resin and each filter tube was again washed five times with nanopure $H_2O$. CML and pentosidine were then eluted into 13×100 mm glass tubes with three consecutive additions of 1 mL 4 M $NH_4OH$; extracts were dried down under $N_2$ at 50°C and 15-20 psi for 2-3 hours in a Zymark Turbo Vap water bath. After drying, extracts were reconstituted with 90:10 $H_2O$:acetonitrile with 5 mM perfluoropentanoic acid (NFPA), vortexed for two min, filtered into 96-well collection plates, and stored at 4°C until analysis.

For the quantification of AGEs in bone, 60mg of each bone sample (crushed in liquid $N_2$) was transferred into borosilicate glass tubes and hydrolyzed, as above. Following hydrolysis, bone hydrolysates were centrifuged at 12,000 rpm for 20 min. Bone hydrolysates were divided into duplicates and were extracted, dried, and reconstituted, as described above. Results of bone extracts were normalized to collagen content in each sample, which was measured using the hydroxyproline assay kit (Sigma-Aldrich, Saint Louis, MO) according to manufacturer's instructions.

For liquid chromatography–tandem mass spectrometry (LC-MS/MS), Sciex API 5000 mass spectrometer utilizing an electrospray ionization source in positive ion mode was used in combination with a Cohesive

TLX4 liquid chromatography system. Ion-pairing chromatography was performed on a Phenomenex Synergi 4µ, Max RP 80A, 2.0×150 mm analytical column with a $C_{12}$, 4×2 mm guard cartridge (Phenomenex). Mobile phases were prepared using NFPA as the ion-pairing agent. Mobile Phase A contained 5 mM NFPA in 90:10 $H_2O$:acetonitrile, whereas Mobile Phase B consisted of 5 mM NFPA in 10:90 $H_2O$:acetonitrile. The liquid chromatography method is detailed in Supplemental Table 2. The total method duration was 19.25 min, with analyte retention times of ~7.3 min for CML, and ~8.8 min for pentosidine. Flow was diverted from the mass spectrometer for the first five min of chromatography to prevent contamination. Ionization was performed in positive mode with multiple reaction monitoring transitions. Mass transitions and compound parameters used for CML and pentosidine and the associated internal standards are included in Supplemental Table 3, whereas source and gas settings are provided in Supplemental Table 4. The QC and precision characteristics of the LC-MS/MS method have been reported previously (9). The average of the duplicates for CML and pentosidine was used in analyses.

*Real-time quantitative polymerase chain reaction (rt-qPCR) analysis.* Osteocyte-enriched cell preparations were generated as described in *Mouse tissue collection and assessments*, immediately homogenized in QIAzol Lysis Reagent (QIAGEN, Valencia, CA), and stored at -80°C for subsequent RNA extraction, cDNA synthesis, and targeted gene expression measurements of mRNA levels by rt-qPCR, as described (1-3). Total RNA was extracted according to the manufacturer's instructions using QIAzol Lysis Reagent followed by purification with RNeasy Mini Columns (QIAGEN, Valencia, CA). On-column RNase-free DNase solution (QIAGEN, Valencia, CA) was then applied to degrade potentially contaminating genomic DNA. RNA purity/quantity was confirmed using a Nanodrop spectrophotometry (Thermo Fisher Scientific, Wilmington, DE). Standard reverse transcriptase was performed using the High-Capacity cDNA Reverse Transcription Kit (Applied Biosystems by Life Technologies, Foster City, CA). Transcript mRNA levels were determined by rt-qPCR on the ABI Prism 7900HT Real Time System (Applied Biosystems, Carlsbad, CA) using, for example, murine TaqMan assays (Thermo Fisher Scientific, Wilmington, DE) to measure $p16^{Ink4a}$ (*Cdkn2a*) and $p21^{Cip1}$ (*Cdkn1a*), as described (1, 2). In addition, because RNA levels were low, and thus the yields of total RNA needed to run in-depth rt-qPCR analyses were limited, the WT-OvationTM Pico RNA amplification system (NuGEN Technologies Inc., San Carlos, CA) was used to synthesize µg quantities of amplified cDNA starting with relatively low total RNA inputs (500 pg to 50 ng), as described previously by our group (10). This well-validated linear amplification system provides both 3'-initiated and random primed amplification and maintains relative representation of each transcript species from the original sample during and after amplification (11). Amplification of cDNA was followed by measurements of transcript mRNA levels of all other genes with SYBR green (QIAGEN, Valencia, CA) as the detection method, as described (1). The mouse primer sequences, designed using Primer Express Software Version 3.0 (Applied Biosystems), for the genes measured by SYBR green are provided in Supplemental Table 5. As done previously (1, 2), input RNA variations were normalized using a panel of five reference genes (*Actb, Hprt, Polr2a, Tbp, Tub1a*) from which the three most stable housekeeping genes were determined by the geNorm algorithm (http://medgen.ugent.be/~jvdesomp/genorm/) (12, 13), followed by the PCR Miner algorithm (14) to adjust for variability in amplification efficiency. For each sample, the median cycle threshold (Ct) of each gene (run in triplicate) was normalized to the geometric mean of the median Ct of the three most stable reference genes, which was determined using the following geNorm algorithm: $2^{(\text{reference Ct} - \text{gene of interest Ct})}$. The ΔCt for each gene was used to calculate the relative mRNA expression changes for each sample. Genes with Ct values >35 were considered – Not Expressed (NE), as done previously (1). The murine primer sequences used are provided in Supplemental Table 5.

*Senescence-associated distension of satellites (SADS) analysis of osteocytes.* Recent work by our group (1-3), has demonstrated via fluorescence in situ hybridization (FISH) that senescent osteocytes display large-scale unraveling of peri-centromeric satellite heterochromatin DNA, termed SADS (15), a hallmark feature of senescent cells that, in addition to senescent osteocytes in bone, has been detected in senescent cells from various other tissues (15-17). As described previously (1-3), the SADS assay was performed on

non-decalcified right mouse tibia sections by FISH to measure SADS in osteocytes of the diaphyseal cortex. Following 4% paraformaldehyde (PFA) crosslinking of tibia sections for 20 min, sections were washed three times (five minutes each in PBS), and dehydrated in graded (70%, 90%, and 100% – three min each) EtOH. Sections were then dried briefly, denatured for 10 min at 80°C in hybridization buffer: 0.1M Tris (pH 7.2), 25mM $MgCl_2$, 70% formamide (Sigma-Aldrich, Saint Louis, MO), 5% blocking reagent (Roche) with 1.0 μg/mL of Cy3-labelled (F3002) CENPB-specific (ATTCGTTGGAAACGGGA) peptide nucleic acid (PNA) probe (Panagene Inc., Korea), followed by dark room hybridization for two hours at RT. Tibia sections were then washed and mounted with vectashield DAPI-containing mounting media (Life Technologies). Confocal microscopy was subsequently performed at the Mayo Clinic Microscopy and Cell Analysis Core to visualize SADS (*i.e.,* decondensed/elongated centromeres), the number of which in each osteocyte was determined in a blinded fashion; a senescent osteocyte was defined using the established cut-off of ≥4 SADS per cell (1, 2).

## Supplemental References


1. Farr JN, Fraser DG, Wang H, Jaehn K, Ogrodnik MB, Weivoda MM, et al. Identification of Senescent Cells in the Bone Microenvironment. *J Bone Miner Res.* 2016;31(11):1920-9.
2. Farr JN, Xu M, Weivoda MM, Monroe DG, Fraser DG, Onken JL, et al. Targeting cellular senescence prevents age-related bone loss in mice. *Nat Med.* 2017;23(9):1072-9.
3. Farr JN, Rowsey JL, Eckhardt BA, Thicke BS, Fraser DG, Tchkonia T, et al. Independent Roles of Estrogen Deficiency and Cellular Senescence in the Pathogenesis of Osteoporosis: Evidence in Young Adult Mice and Older Humans. *J Bone Miner Res.* 2019;34(8):1407-18.
4. Akhter MP, Otero JK, Iwaniec UT, Cullen DM, Haynatzki GR, and Recker RR. Differences in vertebral structure and strength of inbred female mouse strains. *J Musculoskelet Neuronal Interact.* 2004;4(1):33-40.
5. Ritchie RO, Koester KJ, Ionova S, Yao W, Lane NE, and Ager JW, 3rd. Measurement of the toughness of bone: a tutorial with special reference to small animal studies. *Bone.* 2008;43(5):798-812.
6. Oliver W PGAitfdhaemuladsieJMR-.
7. Carriero A, Bruse JL, Oldknow KJ, Millan JL, Farquharson C, and Shefelbine SJ. Reference point indentation is not indicative of whole mouse bone measures of stress intensity fracture toughness. *Bone.* 2014;69C:174-9.
8. Granke M, Makowski AJ, Uppuganti S, Does MD, and Nyman JS. Identifying Novel Clinical Surrogates to Assess Human Bone Fracture Toughness. *J Bone Miner Res.* 2015;30(7):1290-300.
9. O'Grady KL KS, Farr JN, Bondar OP, Atkinson EJ, Achenbach SJ, Eckhardt BA, Thicke BS, Tweed AJ, Volkman TL, Drake MT, Hines JM, Singh RJ. Development and Validation of Mass Spectroscopy Assays for Nε-(1-carboxymethyl)-L-Lysine and Pentosidine in Renal Failure and Diabetes. The Journal of Applied Laboratory Medicine. 2020 (In Press).
10. Fujita K, Roforth MM, Atkinson EJ, Peterson JM, Drake MT, McCready LK, et al. Isolation and characterization of human osteoblasts from needle biopsies without in vitro culture. *Osteoporos Int.* 2014;25(3):887-95.
11. Dafforn A, Chen P, Deng G, Herrler M, Iglehart D, Koritala S, et al. Linear mRNA amplification from as little as 5ng total RNA for global gene expression. *Biotechniques.* 2004;37(5):854-7.
12. Radonic A, Thulke S, Mackay IM, Landt O, Siegert W, and Nitsche A. Guideline to reference gene selection for quantitative real-time PCR. *Biochem Biophys Res Commun.* 2004;313:856-62.
13. Vandesompele J, De Preter K, Pattyn F, Poppe B, Van Roy N, De Paepe A, et al. Accurate normalization of real-time quantitative RT-PCR data by geometeric averaging of multiple internal control genes. *Genome Biol.* 2002;3:research0034.1-0-34.11.
14. Zhao S, and Fernald RD. Comprehensive algorithm for quantitative real-time polymerase chain reaction. *J Comput Biol.* 2005;12(8):1047-64.
15. Swanson EC, Manning B, Zhang H, and Lawrence JB. Higher-order unfolding of satellite heterochromatin is a consistent and early event in cell senescence. *J Cell Biol.* 2013;203(6):929-42.
16. Ogrodnik M, Miwa S, Tchkonia T, Tiniakos D, Wilson CL, Lahat A, et al. Cellular senescence drives age-dependent hepatic steatosis. *Nat Commun.* 2017;8:15691.
17. Ogrodnik M, Zhu Y, Langhi LGP, Tchkonia T, Kruger P, Fielder E, et al. Obesity-Induced Cellular Senescence Drives Anxiety and Impairs Neurogenesis. *Cell Metab.* 2019;29(5):1061-77 e8.

# Supplemental Figures and Figure Legends

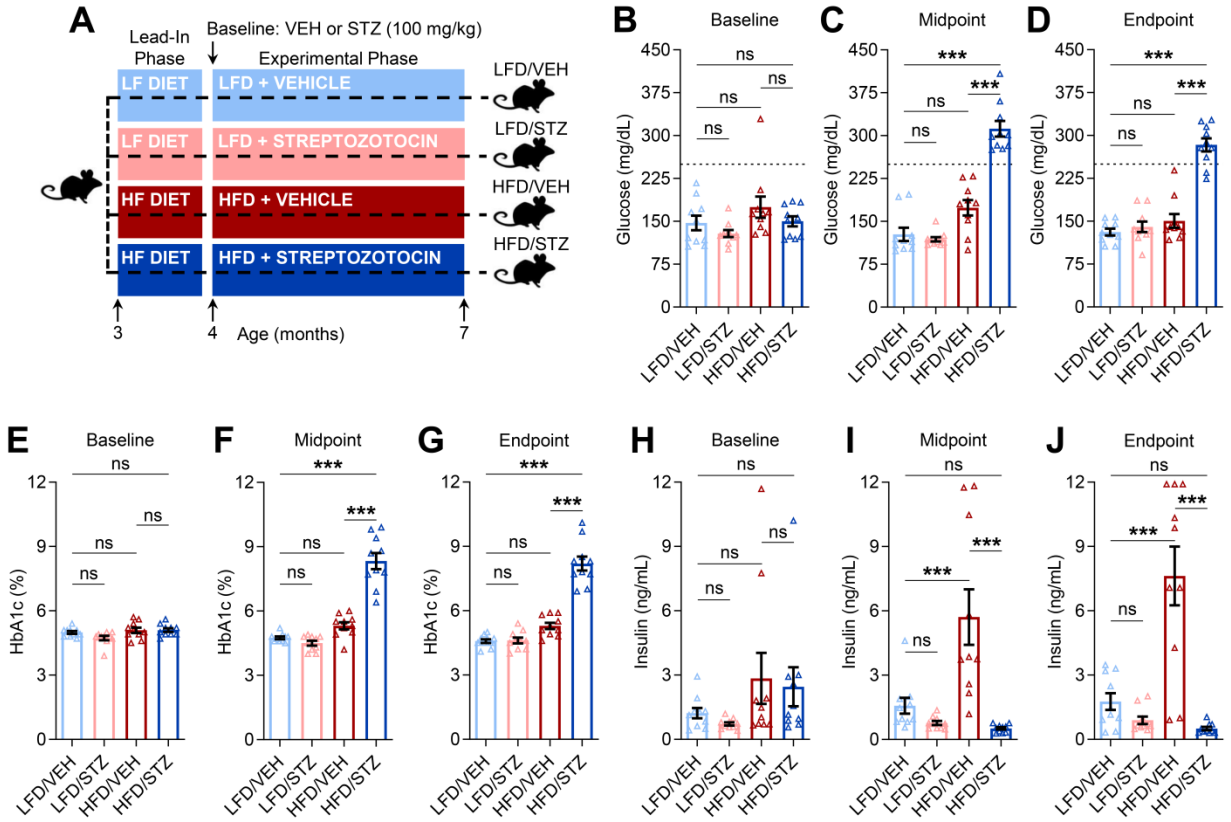


**Supplemental Figure 1. Metabolic characteristics of the HFD/STZ mouse model of T2D.** (**A**) Schematic of the study design depicting male C57BL/6 mice randomized to either LFD (10% kcal from fat) or HFD (60% kcal from fat) for one month (Lead-In phase) followed by treatment (at Baseline) with either VEH or STZ and follow-up for three months (Experimental phase) out to seven months of age (Endpoint): LFD/VEH; LFD/STZ; HFD/VEH; HFD/STZ (n=10/group). Circulating serum glucose (mg/dL) levels at (**B**) Baseline (age 4 months), (**D**) Midpoint (age 5.5 months), and (**D**) Endpoint (age 7 months). Circulating HbA1c (%) levels at (**E**) Baseline, (**F**) Midpoint, and (**G**) Endpoint. Circulating serum insulin (ng/mL) levels at (**H**) Baseline, (**I**) Midpoint, and (**J**) Endpoint. For all analyses, n=10/group. Data represent Mean ± SEM (error bars). *****$p < 0.05$; ******$p < 0.01$; *******$p < 0.001$ (one-way ANOVA with post-hoc Tukey correction for multiple comparisons). Abbreviations: HFD = high-fat diet; STZ = streptozotocin; T2D = type 2 diabetes; LFD = low-fat diet; VEH = vehicle.

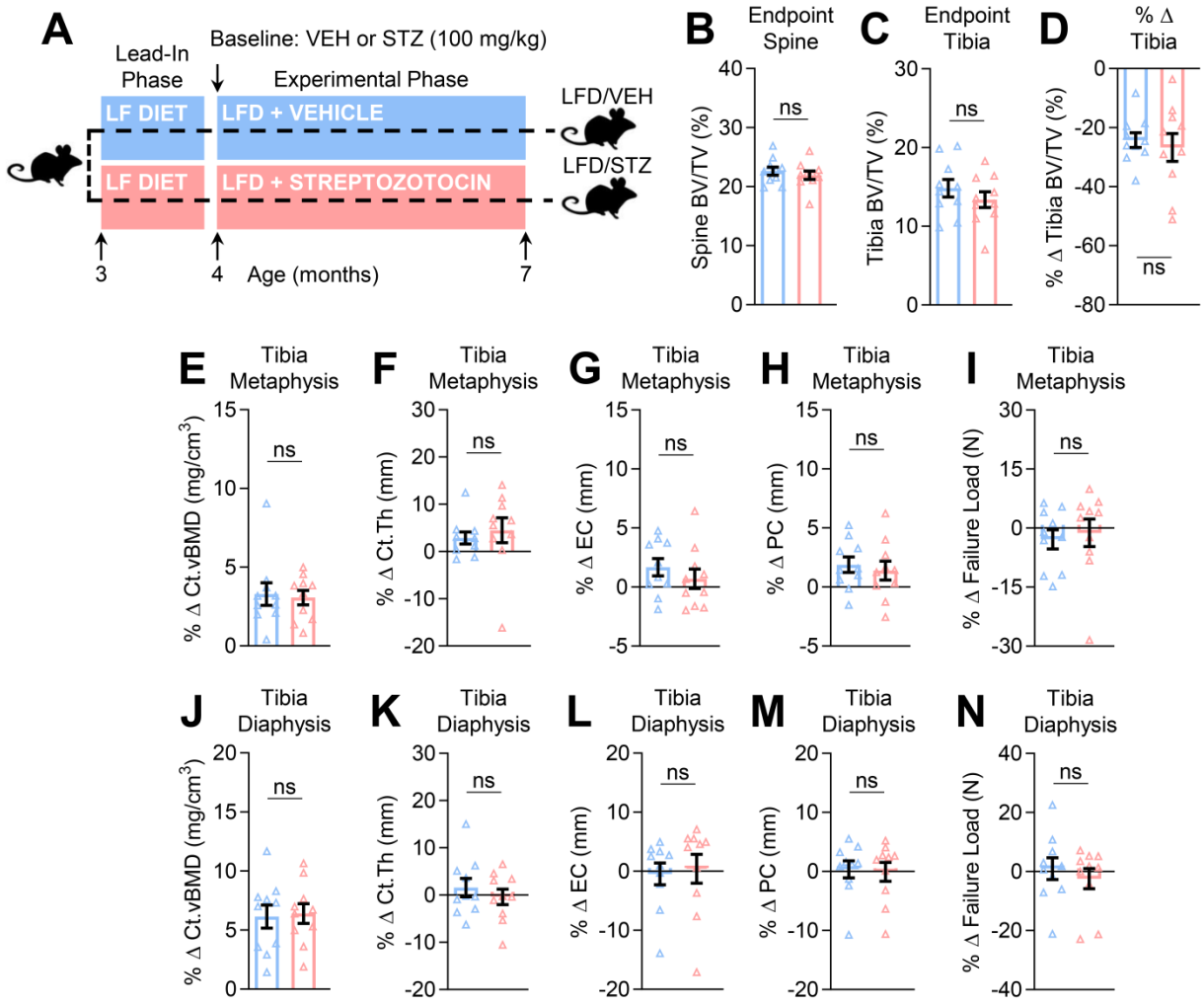


**Supplemental Figure 2. A relatively low dose of streptozotocin (STZ) in the absence of high-fat diet has no substantial effects on bone microarchitecture in mice.** (**A**) Schematic of the study design depicting male C57BL/6 mice randomized to LFD (10% kcal from fat) for one month (Lead-In phase) followed by treatment (at Baseline) with either VEH or STZ and follow-up for three months (Experimental phase) out to seven months of age (Endpoint): LFD/VEH; LFD/STZ (n=10/group). Quantification of micro-computed tomography (µCT)-derived trabecular bone volume fraction (BV/TV; %) assessed *ex vivo* at the lumbar spine (**B**) and tibia metaphysis (**C**) at study Endpoint. (**D**) Percentage change (% Δ) in trabecular BV/TV at the tibia metaphysis assessed by longitudinal *in vivo* µCT analysis (at Baseline and Endpoint). Longitudinal percentage changes (% Δ) in (**E**) cortical volumetric bone mineral density (Ct.vBMD, mg/cm$^3$), (**F**) cortical thickness (Ct.Th, mm), (**G**) endocortical circumference (EC, mm), (**H**) periosteal circumference (PC, mm), and (**I**) micro-finite-element analysis (µFEA)-derived failure load (N, Newton [*i.e.,* an index of bone strength] at the tibia metaphysis. Longitudinal percentage changes (% Δ) in (**J**) Ct.vBMD (mg/cm$^3$), (**K**) Ct.Th (mm), (**I**) EC (mm), (**M**) PC (mm), and (**N**) µFEA-derived failure load (N) at the tibia diaphysis. Data represent Mean ± SEM (error bars). ns = $p \geq 0.05$ (independent samples *t*-Test). Abbreviations: STZ = streptozotocin; LFD = low-fat diet; VEH = vehicle; ns = not significant.

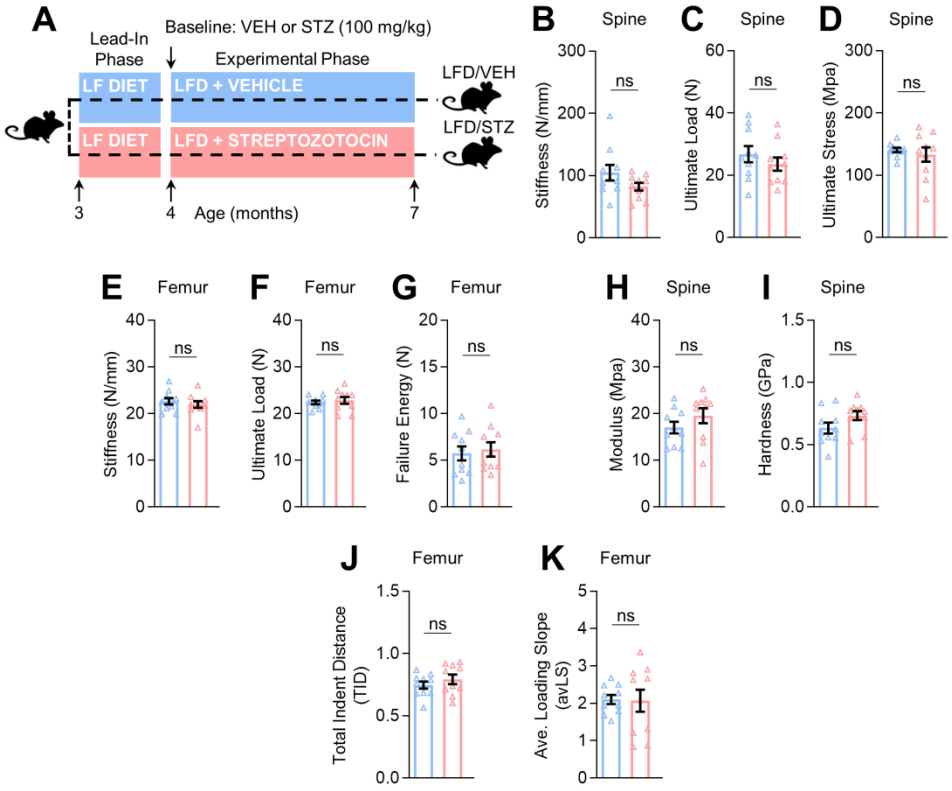


**Supplemental Figure 3. A relatively low dose of streptozotocin (STZ) in the absence of high-fat diet has no substantial effects on bone quality in mice.** (**A**) Schematic of the study design depicting male C57BL/6 mice randomized to LFD (10% kcal from fat) for one month (Lead-In phase) followed by treatment (at Baseline) with either VEH or STZ and follow-up for three months (Experimental phase) out to seven months of age (Endpoint): LFD/VEH; LFD/STZ (n=10/group). Comparisons between the groups at study Endpoint (seven months of age) of bone biomechanical properties (assessed by compression testing) at the lumbar vertebrae, including (**B**) stiffness (N/mm), (**C**) ultimate load (N), and (**D**) ultimate stress (MPa). Endpoint comparisons of bone biomechanical properties (assessed by three-point bending) at the femur midshaft, including (**E**) stiffness (N/mm), (**F**) ultimate load (N), and (**G**) failure energy (N). Endpoint comparisons of bone material properties (assessed by nanoindentation) at the lumbar vertebrae, including (**H**) modulus (GPa) and (**I**) hardness (GPa). Endpoint comparisons of indices of bone material properties (assessed by reference point microindentation) at the femur diaphysis, including (**J**) total indentation distance (TID) and (**K**) average loading slope (avLS). Data represent Mean ± SEM (error bars). ns = $p \geq 0.05$ (independent samples *t*-Test). Abbreviations: STZ = streptozotocin; LFD = low-fat diet; VEH = vehicle; ns = not significant.

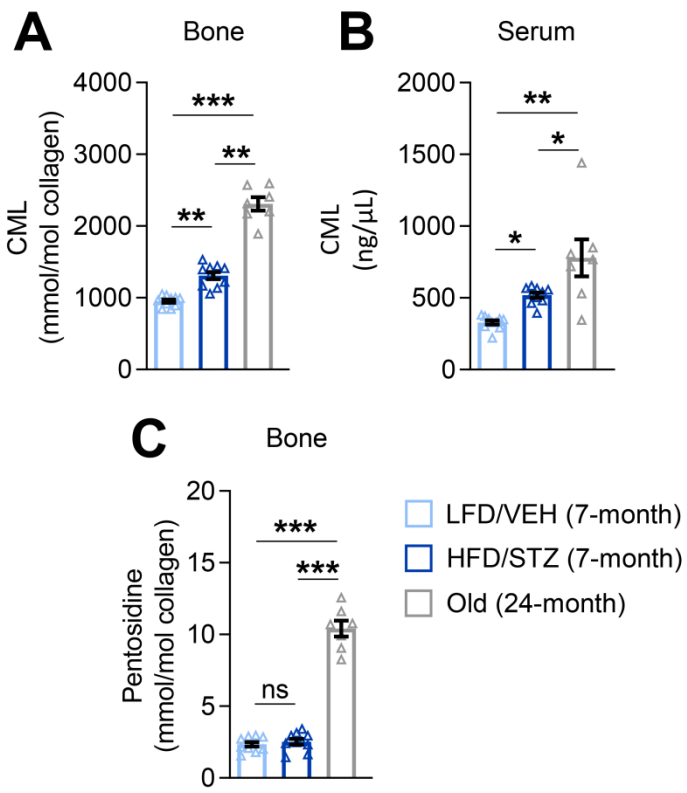


**Supplemental Figure 4. Comparisons of advanced glycation endproducts (AGEs) among control (LFD/STZ, n=10), young (7-month) adult T2D (HFD/STZ, n=10), and old (24-month, n=7) non-diabetic mice.** $N^{\varepsilon}$-(1-carboxymethyl)-L-Lysine (CML) levels in (**A**) bone tissue (mmol/mol collagen) and (**B**) serum (ng/µL) samples. (**C**) Pentosidine levels in bone tissue samples (mmol/mol collagen); note that pentosidine levels were detected at low to non-detectable levels in serum (data not shown). Data represent Mean ± SEM (error bars). ns = $p \geq 0.05$; ***p* < 0.05; ****p* < 0.01; *****p* < 0.001 (one-way ANOVA with post-hoc Tukey correction for multiple comparisons). Abbreviations: HFD = high-fat diet; STZ = streptozotocin; T2D = type 2 diabetes; LFD = low-fat diet; VEH = vehicle; ns = not significant.

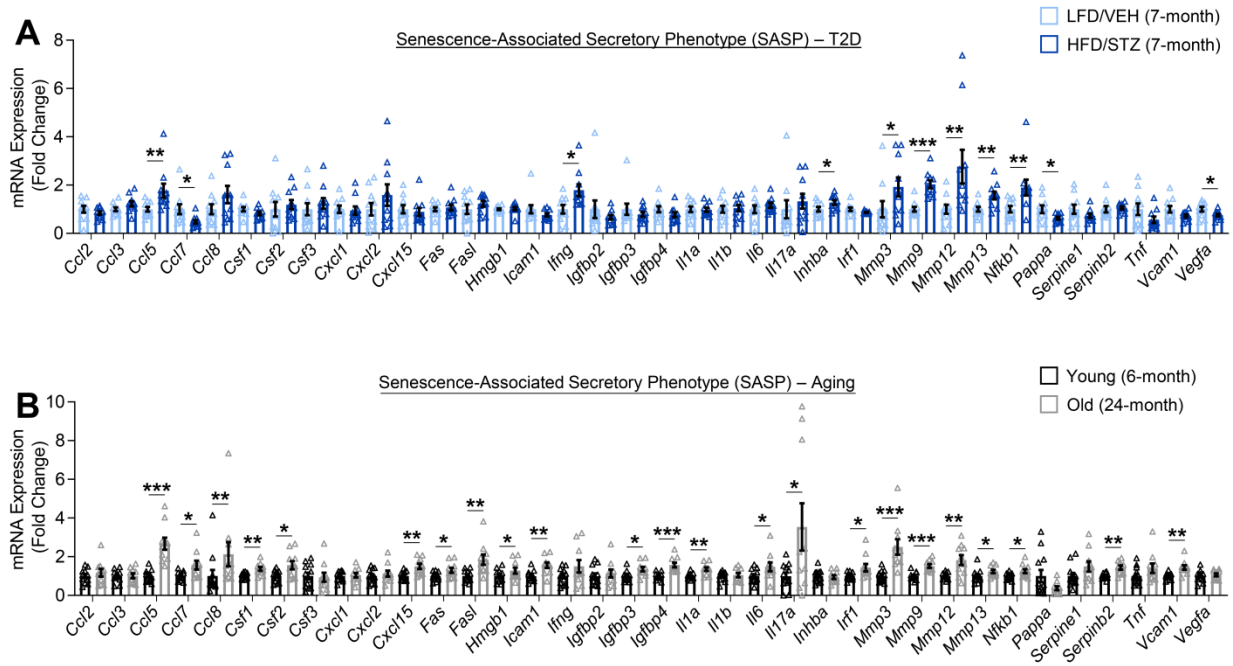


**Supplemental Figure 5. Fold-change comparisons of the senescence-associated secretory phenotype (SASP) in bone between young (7-month) adult LFD/VEH versus T2D (HFD/STZ, n=10) and young (6-month, n=12) adult normal chow-fed wild-type (WT) versus old (24-month, n=10) non-diabetic normal chow-fed WT mice.** *In vivo* T2D- and old-age-associated fold changes in mRNA expression of 36 established SASP factors in bone samples. Data represent Mean ± SEM (error bars). *****$p < 0.05$; ******$p < 0.01$; *******$p < 0.001$ (independent samples *t*-test or Wilcoxon rank-sum test, as appropriate). Abbreviations: SASP = senescence-associated secretory phenotype (SASP); HFD = high-fat diet; STZ = streptozotocin; T2D = type 2 diabetes; LFD = low-fat diet; VEH = vehicle. Young versus Old data are reproduced from (Farr et al. *J Bone Miner Res* 31(11):1920-9, 2016).

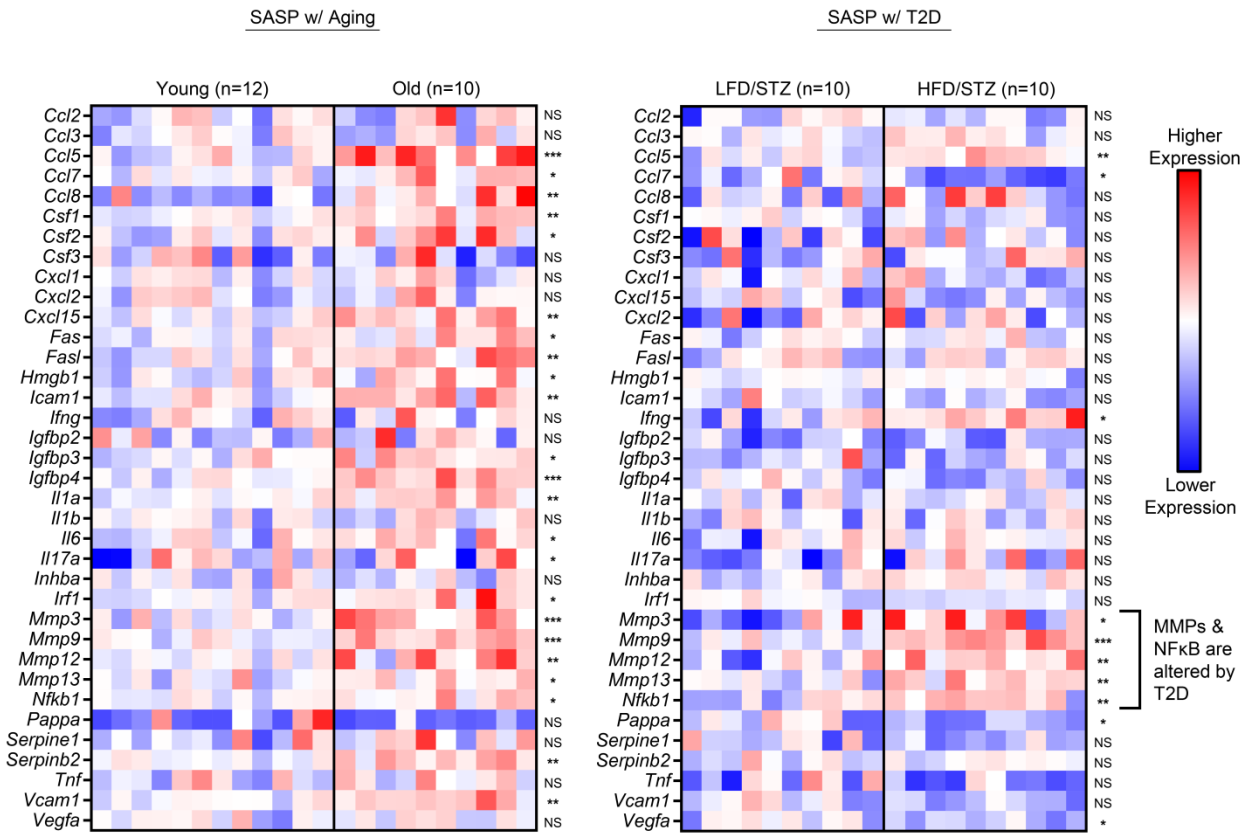


**Supplemental Figure 6. Heat maps of the SASP in bone with aging versus T2D.** Heat maps showing comparisons of the SASP in bone tissue samples of C57BL/6 mice in the setting of aging (Young [n=12] versus Old [n=10]) and T2D (Young LFD/VEH [7-month, n=10] versus T2D [HFD/STZ, n=10]). Note that aging is associated with uniform higher expression of SASP factors in bone, whereas T2D is characterized by a unique SASP, including higher levels of matrix metalloproteinases (MMPs – *Mmp3*, *Mmp9*, *Mmp12*, and *Mmp13*) as well as *NFκB* in bone. *$p < 0.05$; **$p < 0.01$; ***$p < 0.001$ (independent samples *t*-test or Wilcoxon rank-sum test, as appropriate). Abbreviations: SASP = senescence-associated secretory phenotype (SASP); HFD = high-fat diet; STZ = streptozotocin; T2D = type 2 diabetes; LFD = low-fat diet; VEH = vehicle; NS = Not Significant. Young versus Old data are reproduced from (Farr et al. *J Bone Miner Res* 31(11):1920-9, 2016).

## Supplemental Tables

**Supplemental Table 1.** Composition of mouse research diets (% kcal)

| | Low-Fat Diet (LFD) | High-Fat Diet (HFD) |
|---|---|---|
| Fat | 10% | 60% |
| Protein | 20% | 20% |
| Carbohydrate | 70% | 20% |
| Energy Density (kcal/g) | 3.8 | 5.2 |

LFD: https://www.researchdiets.com/formulas/d12450j
HFD: https://www.researchdiets.com/formulas/d12492

**Supplemental Table 2.** Summary of the liquid chromatography method

| Step | Duration (s) | Flow (mL/min) | Gradient | % Mobile Phase A | % Mobile Phase B |
|---|---|---|---|---|---|
| 1 | 150 | 0.35 | Step | 100 | 0 |
| 2 | 120 | 0.35 | Ramp | 60 | 40 |
| 3 | 345 | 0.20 | Step | 60 | 40 |
| 4 | 30 | 0.35 | Ramp | 0 | 100 |
| 5 | 180 | 0.35 | Step | 0 | 100 |
| 6 | 30 | 0.35 | Ramp | 100 | 0 |
| 7 | 300 | 0.35 | Step | 100 | 0 |

**Supplemental Table 3.** Multiple reaction monitoring mass transitions and compound parameters

| Analyte | Q1 Mass (Da) | Q3 Mass (Da) | DP (volts) | CE (volts) |
|---|---|---|---|---|
| CML 1 | 205.0 | 84.0 | 150.0 | 60.0 |
| CML-d4 1 | 209.0 | 88.1 | 150.0 | 60.0 |
| CML 2 | 205.0 | 130.2 | 150.0 | 27.0 |
| Pentosidine 1 | 379.5 | 135.2 | 180.0 | 67.0 |
| Pentosidine-d3 1 | 382.5 | 138.2 | 180.0 | 67.0 |
| Pentosidine 2 | 379.5 | 187.2 | 180.0 | 52.0 |
| Pentosidine-d3 2 | 382.5 | 190.2 | 180.0 | 52.0 |

| **Supplemental Table 4.** Source and gas settings | |
|---|---|
| **Ionization** | **Positive** |
| Collision Gas | 4 |
| Curtain Gas | 35 |
| Ion Source Gas 1 | 50 |
| Ion Source Gas 2 | 40 |
| Ionspray Voltage | 5500 |
| Temperature | 700°C |

| **Supplemental Table 5.** Mouse primer sequences. | | | | |
|---|---|---|---|---|
| **#** | **Category** | **Gene** | **Forward Primer Sequence** | **Reverse Primer Sequence** |
| 1 | Osteoblast marker | *Alpl* | CACAGATTCCCAAAGCACCT | GGGATGGAGGAGAGAAGGTC |
| 2 | Osteoblast marker | *Bglap* | CCTGAGTCTGACAAAGCCTTCA | GCCGGAGTCTGTTCACTACCTT |
| 3 | Osteoblast marker | *Col1a1* | GCTTCACCTACAGCACCCTTGT | TGACTGTCTTGCCCCAAGTTC |
| 4 | Osteoblast marker | *Runx2* | GGCACAGACAGAAGCTTGATGA | GAATGCGCCCTAAATCACTGA |
| 5 | Osteoblast marker | *Sp7* | AAGTTCACtTGCCTGCTCTGTT | TGCGCTGATGTTTGCTCAAG |
| 6 | Osteocyte marker | *Dmp1* | TGCTCTCCCAGTTGCCAGAT | AATCACCCGTCCTCTCTTCAGA |
| 7 | Osteocyte marker | *Fgf23* | TCTCCACGGCAACATTTTTG | CTGGCGGAACTTGCAATTCT |
| 8 | Osteocyte marker | *Mepe* | TGCTGCCCTCCTCAGAAATATC | GTTCGGCCCCAGTCACTAGA |
| 9 | Osteocyte marker | *Phex* | CCTTGGCTGAGACACAATGTTG | GCCTTCGGCTGACTGATTTCT |
| 10 | Osteocyte marker | *Sost* | ACTTGTGCACGCTGCCTTCT | TGACCTCTGTGGCATCATTCC |
| 11 | OPG | *Tnfrsf11b* | CCAAGAGCCCAGTGTTTCTT | CCAAGCCAGCCATTGTTAAT |
| 12 | RANKL | *Tnfsf11* | GCTGGGACCTGCAAATAAGT | TTGCACAGAAAACATTACACCTG |
| 13 | SASP | *Ccl2* | GTCTGTGCTGACCCCAAGAAG | TGGTTCCGATCCAGGTTTTTA |
| 14 | SASP | *Ccl3* | TCCCAGCCAGGTGTCATTTT | TTGGAGTCAGCGCAGATCTG |
| 15 | SASP | *Ccl5* | GCCCACGTCAAGGAGTATTTCT | ACAAACACGACTGCAAGATTGG |
| 16 | SASP | *Ccl7* | CCCTGGGAAGCTGTTATCTTCA | CTGATGGGCTTCAGCACAGA |
| 17 | SASP | *Ccl8* | CCACACAGAAGTGGGTCAGTGA | TTCAAGGCTGCAGAATTTGAGA |
| 18 | SASP | *Csf1* | ATTGCCAAGGAGGTGTCAGAA | GGACCTTCAGGTGTCCATTCC |
| 19 | SASP | *Csf2* | CCTTGAACATGACAGCCAGCTA | CACAGTCCGTTTCCGGAGTT |
| 20 | SASP | *Csf3* | CCTGCAGGCTCTATCGGGTAT | ATCCAGCTGAAGCAAGTCCAA |
| 21 | SASP | *Cxcl1* | CCGAAGTCATAGCCACACTCAA | CAAGGGAGCTTCAGGGTCAAG |
| 22 | SASP | *Cxcl2* | TCAAGGGCGGTCAAAAAGTT | CAGTTAGCCTTGCCTTTGTTCA |
| 23 | SASP | *Cxcl15* | TCCATGGGTGAAGGCTACTGT | TTCATTGCCGGTGGAAATTC |
| 24 | SASP | *Fas* | CTGCACCCTGACCCAGAATAC | ACAGCCAGGAGAATCGCAGTA |
| 25 | SASP | *Fasl* | CCGCTCTGATCTCTGGAGTGA | CACGAAGTACAACCCAGTTTCG |
| 26 | SASP | *Hmgb1* | TCCTTCGGCCTTCTTCTTGTT | AGGATGCTCGCCTTTGATTTT |
| 27 | SASP | *Icam1* | GTGGCGGGAAAGTTCCTGTT | GTCCAGCCGAGGACCATACA |
| 28 | SASP | *Ifng* | TTGGCTTTGCAGCTCTTCCT | ATGACTGTGCCGTGGCAGTA |
| 29 | SASP | *Igfbp2* | GCCCCCTGGAACATCTCTACT | GTTGTACCGGCCATGCTTGT |
| 30 | SASP | *Igfbp3* | ACCTGCTCCAGGAAACATCAGT | TTTCCACACTCCCAGCATTG |
| 31 | SASP | *Igfbp4* | GCAACTTCCACCCCAAACAGT | CCTGTCTTCCGATCCACACA |
| 32 | SASP | *Il1a* | AAGAGACCATCCAACCCAGATC | CCTGACGAGCTTCATCAGTTTG |
| 33 | SASP | *Il1b* | TCAGGCAGGCAGTATCACTCA | CACGGGAAAGACACAGGTAGCT |
| 34 | SASP | *Il6* | ACCACGGCCTTCCCTACTTC | TTGGGAGTGGTATCCTCTGTGA |
| 35 | SASP | *Il17a* | GGACTCTCCACCGCAATGAA | GCACTGAGCTTCCCAGATCAC |
| 36 | SASP | *Inhba* | CAGGAAGACACTGCACTTTGA | TTCAGGAAGAGCCACACTTCT |
| 37 | SASP | *Irf1* | CAGCCGAGACACTAAGAGCAAA | GAGAAAGTGTCCGGGCTAACAT |
| 38 | SASP | *Mmp3* | TTGACGATGATGAACGATGGA | GAGCAGCAACCAGGAATAGGTT |
| 39 | SASP | *Mmp9* | TGAGTCCGGCAGACAATCCT | CCCTGGATCTCAGCAATAGCA |
| 40 | SASP | *Mmp12* | GTGCCCGATGTACAGCATCTT | GGTACCGCTTCATCCATCTTG |
| 41 | SASP | *Mmp13* | TGAGGAAGACCTTGTGTTTGCA | GCAAGAGTCGCAGGATGGTAGT |
| 42 | SASP | *Nfkb1* | GGCTTTGCAAACCTGGGAAT | TCCGTGCTTCCAGTGTTTCA |
| 43 | SASP | *Pappa* | CATCTCAGGTGTGTCGAACCA | TGCAAGGATACCAAGCATGCT |
| 44 | SASP | *Serpine1* | GGACACCCTCAGCATGTTCA | CGGAGAGGTGCACATCTTTCT |
| 45 | SASP | *Serpinb2* | TTCCGCATACTGGAAACATCAG | GGATGCGTCCTCAATCTCATC |
| 46 | SASP | *Tnf* | GTTCTGCAAAGGGAGAGTGG | GCACCTCAGGGAAGAGTCTG |
| 47 | SASP | *Vcam1* | GGCTCCAGACATTTACCCAGTT | CATGAGCTGGTCACCCTTGAA |
| 48 | SASP | *Vegfa* | GTACCTCCACCATGCCAAGTG | TGGGACTTCTGCTCTCCTTCTG |
| 49 | Housekeeping | *Actb* | AATCGTGCGTGACATCAAAGAG | GCCATCTCCTGCTCGAAGTC |
| 50 | Housekeeping | *Hprt* | CGTGATTAGCGATGATGAACCA | TCCAAATCCTCGGCATAATGA |
| 51 | Housekeeping | *Polr2a* | CGAATTGACTTGCGTTTCCA | ATGTGCCGTTCCACCTTATAGC |
| 52 | Housekeeping | *Tbp* | CTTCACCAATGACTCCTATGACCC | CGCAGTTGTCCGTGGCTCTCTTA |
| 53 | Housekeeping | *Tuba1a* | GGTTCCCAAAGATGTCAATGCT | CAAACTGGATGGTACGCTTGGT |